JOURNAL OF COMPUTATIONAL PHYSICS 7, 120–133 (1971)

On the Magnitude of the Subgrid Scale Eddy Coefficient

J. W. DEARDORFF

National Center for Atmospheric Research Boulder, Colorado 80302*

Received May 25, 1970

Three-dimensional numerical integrations capable of resolving the energy containing motions at large Reynolds number have tested the nonlinear eddy–viscosity formulation in the two cases when the turbulence is generated by mean shear or by thermal instability. The proportionality constant suggested by Lilly is found to be applicable in the latter case, but a smaller value is found necessary in the presence of mean shear. Spectra of calculated velocity components are shown to deviate from a $k^{-5/3}$ law, as k approaches the grid cutoff wavenumber, in a manner consistent with the application of Reynolds-averaging over grid volumes.

1. INTRODUCTION

With the aid of Reynolds-averaging over finite-difference grid volumes, it is possible with the latest computers to simulate turbulent motions on a grid in three dimensions [1–3] and thereby gain useful information. Eulerian properties of the calculated flow reported in Refs. [1, 2] which closely resemble real turbulence include the irregular everchanging motions, magnitudes and distributions of the turbulence intensities, vertical transport of momentum, velocity autocorrelations and correlation coefficients, and the net stretching of vortex lines. The dispersive nature of the calculated velocities is reported in Ref. [3], along with evaluation of Lagrangian autocorrelation coefficients.

The local Reynolds stresses which arise from the averaging process have so far been simulated by about the crudest of methods: That involving an eddy coefficient with magnitude limited in some way by the size of the averaging domain. When this domain is considered to be the grid volume of a detailed numerical integration, the eddy coefficient K becomes a "subgrid scale" or "SGS" eddy coefficient.

For simulation of three-dimensional turbulence, Lilly [4] has shown that the formulation of Smagorinsky [5] for K is consistent with the existence of a three-

* The National Center for Atmospheric Research is sponsored by the National Science Foundation.

dimensional inertial subrange on scales comparable to and less than the grid interval. The formulation, which allows K to be variable in space and time, is

$$K = (c\Delta)^2 D/\sqrt{2}, \tag{1}$$

where Δ is a representative grid interval, D is the magnitude of the local velocity deformation calculated on the finite-difference grid, and c is the dimensionless constant which forms the main topic of this paper. More specifically, D is given by

$$D = \left[\left(\frac{\delta\bar{u}_i}{\Delta x_j} + \frac{\delta\bar{u}_j}{\Delta x_i}\right)\left(\frac{\delta\bar{u}_i}{\Delta x_j} + \frac{\delta\bar{u}_j}{\Delta x_i}\right)\right]^{1/2}, \tag{2}$$

where summation is implied over $i, j = 1, 2, 3$; the overbar is the Reynolds average over the grid volume (the average is taken to be continuous over space), $\bar{u}_i$ is a calculated velocity component at a grid point, and δ denotes the simplest centered finite difference across the interval $(\Delta x)_j$. (See the Appendix for the finite-difference form of the velocity gradient and of K for the space-staggered velocity grid.) The SGS Reynolds stresses are assumed given by

$$\overline{u_i' u_j'} - \frac{1}{3}\delta_{ij}\overline{u_l' u_l'} = -K\left(\frac{\delta\bar{u}_i}{\Delta x_j} + \frac{\delta\bar{u}_j}{\Delta x_i}\right), \tag{3}$$

where δ_{ij} is the Kronecker delta, and the primes denote the deviation at any point from the Reynolds-averaged value centered at the same point.

2. Theoretical Estimates of c

Although (1) is more applicable to three-dimensional turbulence than to two-dimensional flows, Smagorinsky [5] used formulation (1) for numerical calculations of the large-scale global atmospheric circulation with the value $c = 0.4 = k$, the Karman constant. This value can be arrived at by setting K and D in (1) to their respective values within a "constant-stress" boundary layer,

$$ku_* z_1 = (c\Delta)^2 u_*/(kz_1),$$

where u_* is the friction velocity at the surface and z_1 is the level of application within the "constant-stress" layer. Upon solving for c, we find

$$c = \left(\frac{z_1}{\Delta}\right) k. \tag{4}$$

If the level at which K is desired equals Δ and indeed lies within the "law-of-the-wall" region, and if at this level almost all the calculated velocity deformation is associated with the large-scale mean shear, then (4) is appropriate with $c = k$.

However, one or both of these assumptions is usually grossly violated except, perhaps, at the lowest level of grid points. Thus, (4) has no particular relevance above this level in a numerical calculation.

Lilly [4] has estimated c with approximate knowledge of the Kolmogorov inertial-subrange constant α. He assumed that isotropic turbulence with such an inertial subrange was present in the problem being simulated numerically on scales both much greater and much less than the grid interval Δ. He also assumed $\Delta x = \Delta y = \Delta z = \Delta$, and took the Reynolds averaging volume to be Δ^3. He found that

$$c \cong 0.23\alpha^{-3/4}.$$

For $\alpha = 1.41$, an average value from the measurements of Pond et al. [6] for the three-dimensional energy-spectrum constant, it follows that $c = 0.176$. However, this value did not take into account that D in (1) is obtained as a finite difference. When this fact was taken into account, with velocity differences taken across *single* grid intervals, Lilly [7] found a 25% increase, giving $c = 0.22$. A more recent, revised value of c by Lilly (unpublished) using $\alpha = 1.50$ is

$$c = 0.20. \tag{5}$$

Of course, this value of c could not be recommended for numerical integrations in which the finite-difference techniques contain significant numerical instabilities or built-in smoothing. An example where it would not apply is the Lax–Wendroff method [8] in which intrinsic damping occurs even in the absence of any viscous terms. Another example is the "MAC" method [9] where forward time steps are used with respect to the advective terms. That method is absolutely unstable (Thompson [10, p. 68], Hirt [11]) unless the viscosity is sufficiently large. Some examples which *are* suitable, however, having essentially neutral numerical stability, include the methods recommended by Lilly [12] and Williams [13]. In both these methods, and independently in [9], the approach of Arakawa [14] is used for the finite-differencing of the nonlinear advective terms. Nonlinear instability is thereby avoided. Time differencing is by means of the Adams–Bashforth (see Ref. [12]) or central differencing "leapfrog" technique (see Fischer, Ref. [15]).

3. Three-Dimensional Numerical Estimates of c

The essential techniques recommended by Williams [13] were used independently by Deardorff [1] in a study of turbulent channel flow (plane Poiseuille flow) at large Reynolds number. Here it was found that the use of $c = 0.17$,

which is even smaller than the theoretical value in (5), led to K values sufficiently large to damp the eddies out unless the mean shear became and remained excessively large. Instead, the value

$$c = 0.10 \tag{6}$$

was found to be the best single value applying throughout the flow, using the measurements of Laufer [16] as a standard for comparison. In the computations, a total of $24 \times 14 \times 20$ grid intervals were used in the respective downstream (x), cross-stream (y), and normal or vertical (z) directions. The grid points closest to the wall lay well outside of the laminar sublayer but within an assumed "law-of-the-wall" region. The dimensionless grid intervals, scaled by the full channel height, were $\Delta x = 0.125$, $\Delta y = 0.05 = \Delta z$. In (1), Δ was taken to be

$$\Delta = (\Delta x \cdot \Delta y \cdot \Delta z)^{1/3}. \tag{7}$$

The same methods were also used on a different problem—the turbulent flow within a neutral planetary (rotating) boundary layer [2]. The same grid network and dimensionless grid intervals were used, scaled, however, with the approximate height of the planetary boundary layer, with the exception that Δy was increased to 0.071. Again the value $c = 0.10$ gave reasonable results although in this problem a mean shear exists in not just one but two velocity components.

In more recent numerical integrations not yet reported, the number of grid intervals was nearly doubled: $40 \times 20 \times 20$, and the dimensionless grid intervals set at $\Delta x = \Delta y = 0.10$, $\Delta z = 0.05$. Numerical techniques were the same as in Refs. [1–3] except that the pressure was obtained exactly from a fast Fourier-transform inversion, rather than approximately from overrelaxation. Also, temperature was included as an additional but passive variable, located at the same grid points as pressure. This time, examination of one-dimensional spectra disclosed some piling up of energy on the $2\Delta x$ scale. By increasing c from 0.10 to 0.13 this was eliminated, although at the lowest interior grid points within the "constant-stress" layer the value of c was maintained at about 0.10. At this level ($z_1 = \Delta z/2$ for a "staggered" velocity grid) no piling up of energy had occurred, and although (4) and (7) gave $c = 0.13$, this value was an appreciable overestimate. Even at this small height a significant fraction (about 50%) of the velocity deformation D was associated with fluctuating local gradients. The value $c = 0.10$ at this level was therefore more correct. It is probable that had $c = 0.13$ been used in the interior and $c = 0.10$ near the boundaries in the channel-flow problem, results would have been as favorable as using $c = 0.10$ throughout. However, the discrepancy between $c = 0.13$ and Lilly's value $c = 0.20$ was still perplexingly large.

Additional integrations with the grid network of greater resolution were made

for the case of an unstably stratified planetary boundary layer in which the temperature was an active, rather than passive, variable. The degree of thermal instability was relatively small, with $-H/L = 4.5$, where H is the height of the convecting region and L the Monin–Obukhov length. However, the vertical mixing was much more pronounced, and very little mean shear remained in the interior, after a statistically steady state was achieved, in comparison with the amounts in the neutral planetary boundary layer. It was found that excess energy accumulated near the $2\Delta x$ and $2\Delta y$ scales until c had been increased to about 0.21. (Spurious energy which piled up when using a c value too small had to be removed by selective filtering before continuing the integration.) With this value of c, the energy cascading towards higher wavenumbers was removed (transferred to the subgrid scale) at the proper rate that a reasonable energy spectrum existed at higher wavenumbers (see Section 4), and no further filtering was necessary. At the grid points nearest the lower boundary, c was again maintained somewhat smaller than the value prescribed by (4). The difference between the value of c used in the interior, 0.21, and that derived by Lilly, $\sim$0.20, for isotropic turbulence, is well within the limits of uncertainty of either method of estimating its proper value.

It is therefore being suggested here that this near coincidence of c values is not accidental, and that turbulence generated by a shear flow is a rather special case requiring a smaller magnitude for c.

Average vertical distributions of K for the four cases discussed are shown in Fig. 1: Channel flow and the neutral planetary boundary layer (PBL) both having $c = 0.10$ throughout; the neutral and weakly unstable PBL with improved resolution having larger values of c outside of the "constant-stress" region. The channel-flow K distribution is symmetric about $z/H = 0.5$. In the PBL distributions K decreases monotonically with height except in the unstable PBL where a slight increase near the top is associated with impinging thermal plumes and enhanced values of $|\, \partial\bar{w}/\partial z \,|$. At $z = H$ the condition $\bar{w} = 0$ was specified in all cases, which is unduly restrictive in its simulation of a penetrable inversion base.

In the two cases where $c = 0.10$ throughout (dashed curves of Fig. 1) the distribution is nearly discontinuous in passing away from the wall region. In the other two cases with c larger outside of the "constant-stress" region, the profiles seem more continuous and perhaps more correct. In the case of the weakly unstable PBL, K in the "constant-stress" layer was specified to be about 1.3 times its neutral value. A somewhat larger factor of enhancement of 1.5 can be obtained from the diabatic profile theory of Businger and Dyer [17] with the knowledge that $z_1 = \Delta z/2 = H/40$.

These SGS K values should not be confused with the more usual "total" eddy coefficients which arise from large-scale horizontal averaging or from ensemble averaging. The "total" eddy coefficient $\mathscr{K}_{xz}$, for example, can be split into the

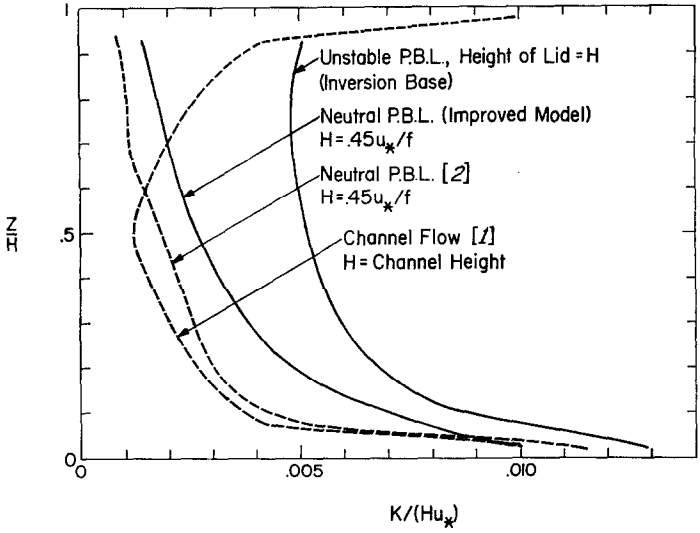

FIG. 1. Vertical distribution of average subgrid-scale K values for four cases indicated. K is made dimensionless by the product of H, the total height, and u_*, the surface friction velocity.

part associated with the calculated, resolvable turbulence, and the part associated with the unresolvable SGS motions as follows:

$$\mathscr{K}_{xz} = \frac{-\langle \overline{uw} \rangle}{\partial \langle \bar{u} \rangle / \partial z} = \frac{-\langle \bar{u}\bar{w} \rangle}{\partial \langle \bar{u} \rangle / \partial z} - \frac{\langle \overline{u'w'} \rangle}{\partial \langle \bar{u} \rangle / \partial z} \cong \frac{-\langle \bar{u}\bar{w} \rangle}{\partial \langle \bar{u} \rangle / \partial z} + \langle K \rangle,$$

where the angular brackets represent an ensemble or horizontal average of large scale. The directly calculated portion of the total eddy coefficient may become up to an order of magnitude larger than the SGS eddy coefficient $\langle K \rangle$ [2], and for the unstable PBL can even be negative.

It is interesting to note that (1) appears to apply for the case of thermal convection without any modification, i.e., without any added factor of enhancement containing lapse rate or heat flux. Instead, enhancement of K occurs automatically when local velocity gradients of small scale are enhanced, as could be caused by thermal convection. That formulation (1) should be applicable for unstable stratification is consistent with the fact that a $\kappa^{-5/3}$ inertial subrange has frequently been reported [18, 19] for this case. The stability of c was tested in further numerical integrations for a more vigorously unstable PBL with $-H/L = 45$. Although dimensionless velocities were of considerably larger magnitude than for the case $-H/L = 4.5$, the same value $c = 0.21$ was found to yield very reasonable results judging from spectra at the larger wavenumbers as well as from the appearance of the energy bearing motions.

Local enhancement of calculated K values may be seen in a cross-sectional view in Fig. 2 of one of 40 y–z planes in the slightly unstable PBL with $-H/L = 4.5$. Here the fluctuations in velocity, potential temperature, and pressure are also shown at the same time. Velocity components are made dimensionless by u_*, pressure by ρu_*^2, and Θ represents the surface-to-air potential temperature difference made dimensionless by the surface kinematic heat flux divided by u_*. Except for K values, the horizontal means have been removed. Note that Θ is negative in warm air and positive in cool air, and that K is generally greater in ascending warm currents or near their edges than elsewhere at the same height.

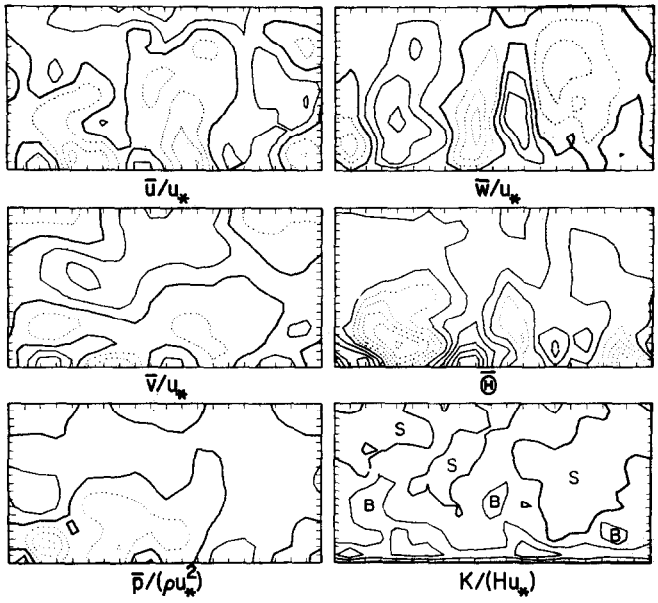

FIG. 2. Contours of velocity components, pressure, dimensionless surface-minus-air potential temperature $\tilde{\Theta}$, and subgrid-scale eddy coefficient K in a y–z plane at a particular time in the statistically steady state of an unstable planetary boundary layer ($-H/L = 4.5$). Except for K, horizontally averaged mean values have been removed from these fields to reveal only the fluctuations. Contour interval for $\tilde{u}/u_*$ and $\tilde{v}/u_*$ is 1.0, for $\tilde{w}/u_*$ is 0.75, for $\tilde{\Theta}$ is 0.30, for $\tilde{p}/(\rho u_*^2)$ is 1.50, and for $K/(Hu_*)$ is 0.003. Regions of small K are labeled S and regions of relatively big K are labeled B. In the other variables, positive or zero contours are solid, negative ones dotted. Dotted contours of $\tilde{\Theta}$, however, refer to relatively warm air and solid contours of $\tilde{\Theta}$ to cool air.

The implication is that the SGS eddies are more intense within these regions, this having been accomplished in nature partly by the upward advection of small scale turbulence from lower levels where its intensity is largest. In the numerical model this appears to have been accomplished partly by upward advection of

local velocity deformation D, upon which K depends, which is generally largest near the lower boundary.

In the case of stable stratification, (1) cannot be expected to hold. Then the spectrum is apt to possess a buoyant-subrange slope steeper than $-5/3$, and the value of c in (5) is probably incorrect. Furthermore, the turbulence may then exist only in patches. No relevant three-dimensional numerical integrations to test the stable case are known to exist.

4. Spectra of (Reynolds-Averaged) Velocities and Temperature

Some one-dimensional spectra calculated from the results of the numerical model of the planetary boundary layer with greater instability ($-H/L = 45$) are shown in Fig. 3. For this particular integration, the number of grid intervals

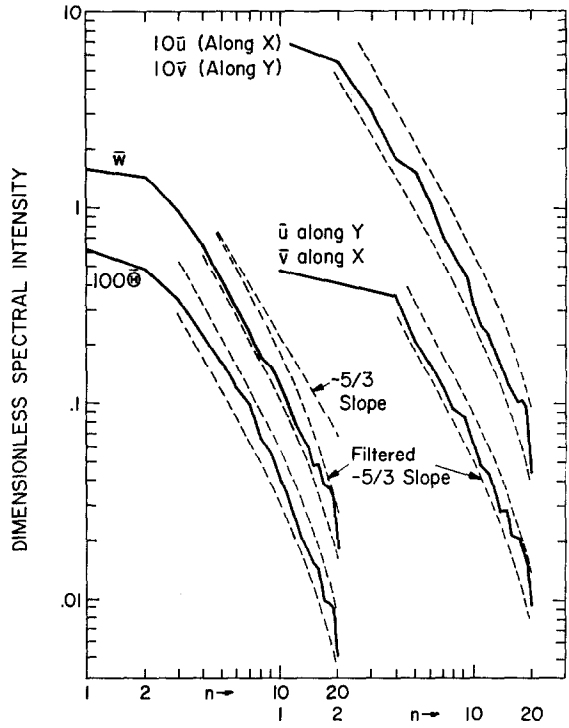

Fig. 3. One-dimensional horizontal spectra of calculated velocity components and of potentia temperature at the level $z/H = 0.475$ within an unstable planetary boundary layer ($-H/L = 45$). Wave $n = 1$ corresponds to the largest possible horizontal wavelength and wave $n = 20$ corresponds to the $2\Delta x$ or $2\Delta y$ wave.

was doubled in the y direction, giving $40 \times 40 \times 20$ grid points within the volume $4H \times 4H \times H$. The nondimensional spectra are averages along horizontal lines at a level about halfway between the surface and the top of the convecting region. The spectra are also averages in time over 10 realizations separated by time intervals of $0.07H/u_*$. Wavelengths extend from $0.2H$ to $4H$, where the height H of the convecting region could be considered to be of order 1 km. The plotted spectral intensities, $\bar{E}(n)/u_*^2$ and $\bar{\Theta}^2(n)$, are related to the more familiar $\bar{E}(\kappa)$ and $\bar{\Theta}^2(\kappa)$ by

$$\frac{\bar{E}(n)}{u_*^2} = \kappa_1 \frac{\bar{E}(\kappa)}{u_*^2} \qquad \text{and} \qquad \bar{\Theta}^2(n) = \kappa_1 \bar{\Theta}^2(\kappa),$$

where $\kappa = 2\pi n/L'$ and $\kappa_1 = \kappa$ at $n = 1$. L' is the length or width of the region between cyclic lateral boundaries. The total variance not associated with a constant value along a line is simply the summation over n of the $\bar{E}(n)$ or $\bar{\Theta}^2(n)$ values on the curves.

The spectral slopes are generally steeper than $-5/3$ over the upper half of wavenumbers, becoming steepest at the grid-cutoff wavenumber $\kappa = \pi/\Delta x$ or $\pi/\Delta y$, corresponding to $n = 20$. This shape is expected when it is realized that it is the *unaveraged* velocity component which is assumed to have a $\kappa^{-5/3}$ spectrum in the vicinity of the cutoff wavenumbers. The Reynolds-averaged velocity components and temperature which are predicted numerically should therefore contain less intensity, especially towards higher wavenumbers, than do the unaveraged variables. Their spectra near the cutoff wavenumbers therefore resemble spectra within a dissipation subrange. Another way of stating this is that the eddy viscosity has taken the place of the molecular viscosity, with the effective dissipation range being shifted far to the left on a spectral plot. With this interpretation, the relevant Reynolds number of the problem is the eddy Reynolds number $R' = u_* H/K$, which had values ranging from about 100 to 1000 in the cases considered. Since $K >>> \nu$, where ν is the kinematic viscosity, it follows that $R' <<< R$, where R is the actual Reynolds number.

An estimate of the one-dimensional spectrum of an inertial-subrange variable which has been Reynolds-averaged over grid volumes is provided by multiplying the $\kappa^{-5/3}$ spectrum by the square of the attentuation factor arising from Reynolds averaging over Δx (or Δy) alone. This factor is $\sin(\kappa\Delta x/2)/(\kappa\Delta x/2)$, (see Ref. [20, p. 12]). Both the $-5/3$ and the filtered $-5/3$ spectra are indicated in Fig. 3. The slope of the latter curve at the cutoff wavenumber is $-11/3$.

The fact that the calculated spectra of Fig. 3 follow a filtered $\kappa^{-5/3}$ curve very closely for $n \geqslant 4$ indicates that the unaveraged spectra of the PBL being modeled would be expected to follow the $\kappa^{-5/3}$ law in this range. Whether or not this range of wavenumbers should be called an "inertial subrange" is debatable, for energy is undoubtedly being fed into the turbulence at all wavenumbers shown. Hence,

the rate of cascade of energy down the spectrum must be considerably greater at $n = 20$ than at $n = 4$. Also, due to the anisotropy in the turbulence energy at heights near $z/H = 0.45$, where the energy of the vertical velocity fluctuations was twice that of either horizontal component, the spectral intensity of $\bar{w}$ and its rate of cascade of energy towards higher wavenumbers is seen to be about twice that for $\bar{u}$ along y or $\bar{v}$ along x for $n \geqslant 4$. (The latter two spectra were identical except for sampling errors, and were averaged together, as was the spectrum of $\bar{u}$ along x with $\bar{v}$ along $\bar{y}$, $\bar{w}$ along x with $\bar{w}$ along y, and $\bar{\Theta}$ along x with $\bar{\Theta}$ along y.) It is also significantly larger than 4/3 times that of $\bar{u}$ along x or $\bar{v}$ along y, this factor of enhancement being expected only if isotropy existed.

Measurements also seem to show the existence of $k^{-5/3}$ spectra under similar conditions of anisotropy within the unstable PBL [19, 21]. As yet, no convincing explanation for this "apparent" inertial subrange is available, nor is it known whether it merges into a true inertial subrange at some large wavenumber or whether anisotropy persists into the molecular-dissipation subrange.

A small but systematic deviation of the spectra from the filtered $-5/3$ curves may be noted at the largest three wavenumbers. Wavenumber 18 seems to contain about 20% too much energy, wavenumber 19 about 30% too much, and wavenumber 20 about 20% too little. This may be some sort of aliasing error. Or, if the spectral estimate for wavenumber 20 were to be doubled to account for the fact that the $2\Delta x$ harmonic contains only the cosine wave, it may indicate that a value of c slightly greater than 0.21 is appropriate.

It may be noted that although the value of $c \cong 0.20$ in (5) was derived under the assumption of local isotropy, the use of the single value $c = 0.21$ for K values occurring in all three equations of motion did not prevent anisotropic $k^{-5/3}$ spectral ranges from occurring. It might be thought that the greater cascade rate for the vertical component of energy than for either of the horizontal components would require a greater value of c in the vertical-component equation of motion. However, the extremely similar shapes of all three velocity spectra in Fig. 3 suggest that a single value of c for all three governing equations is entirely adequate.

The spectrum for temperature, $\bar{\Theta}$, became similar to the velocity spectra at high wavenumbers as in Fig. 3, only after its SGS eddy coefficient K_T had been increased by a factor of three over K for momentum at grid points outside of the "constant-stress" layer. Here K_T is defined by

$$\overline{u_i' \theta'} = -K_T \frac{\partial \bar{\theta}}{\partial x_i}, \tag{7}$$

where θ is the potential temperature. This conclusion held for either the unstable case when $\bar{\theta}$ interacted with $\bar{w}$ or the case when it was a passive scalar within a neutral PBL. Within the "constant-stress" region, however, the two eddy coeffi-

cients were equated, for the case of neutral thermal stability, to be consistent with micro-meteorological measurements [18, p. 105].

The relatively large factor of three for K_T/K in the interior region where the energy containing eddies could be fairly well resolved is qualitatively consistent with the finding of Kraichnan [22] that the relative rate of cascade of scalar variance to higher wavenumbers is markedly greater than the rate for energy cascade in an inertial subrange. However, the accuracy of the empirically derived factor of three cannot yet be stated, it being known only that a factor of two, which had also been tested, was too small.

Although it will probably be many years before digital computers have evolved to the point where spectra from three-dimensional numerical integrations can even begin to compete in range with measured spectra, examination of the numerical spectra is almost indispensible for checking if the magnitudes of K and c are consistent with the assumed size of the Reynolds averaging volume.

5. Conclusions

The formulation of Smagorinsky [5] for the SGS eddy coefficient, with Lilly's approximate value for the relevant constant ($c \cong 0.21$) gives very reasonable results for three-dimensional numerical integrations in which thermal convection is the driving mechanism. If a large-scale velocity shear supplies the energy to the turbulence, then a significantly smaller value ($c \cong 0.13$) seems necessary. Although the reason for this is not yet known, it appears that the dominating presence of a large-scale mean shear has an inhibiting effect upon the inertial cascade rate for a given value of velocity deformation D. An extreme example which illustrates this effect is large-scale shear in the absence of turbulence. Then K should be essentially zero, requiring c to be essentially zero because D has a finite value due to the large-scale shear.

A value of c somewhat smaller than that of the Karman-constant analogy, (4), was found appropriate at grid points within the "constant-stress" layer near a wall or boundary.

The SGS eddy coefficient for a scalar such as temperature was found to be approximately three times larger than that for momentum outside of the unresolvable region nearest the walls or boundary.

Spectra near the cutoff wavenumber are rather sensitive indicators to the magnitude of K or c. It is suggested that c in formulation (1) is too small if the spectra do not behave as in a dissipation subrange as κ approaches its cutoff value, with the slope becoming about $-11/3$ at the cutoff wavenumber in the case when a $\kappa^{-5/3}$ inertial subrange exists in this region for the non-Reynolds-averaged variable. It would be desirable for a theoretical study to be undertaken to determine

more accurately the expected one-dimensional spectrum of a Reynolds-averaged inertial-subrange variable, for various averaging volumes lying within a three-dimensional inertial subrange. This would permit more accurate empirical determinations of c to accompany the desired size of the Reynolds-averaging volume.

APPENDIX. FINITE-DIFFERENCE FORM OF K

The space-staggered finite-difference velocity grid is shown in Fig. 4 in two dimensions, x and y, for simplicity. The method of extension to three dimensions is evident. Here p is the grid-volume averaged pressure, with overbars having been omitted. The eddy coefficients were positioned at the pressure grid points.

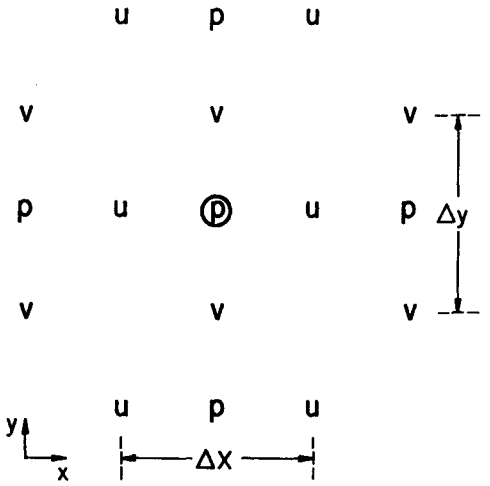

FIG. 4. Relative locations of pressure, p, and of velocity components, u and v, for the space-staggered velocity grid in an x–y plane.

Let the central, circled pressure point be designated by $p(I, J)$, where $x = I\Delta x$ and $y = J\Delta y$. Then the portion of K associated with velocity gradients in the x–y plane was approximated in finite-difference form by

$$
\begin{aligned}
&K(I, J)\\
&= (c\Delta)^2\{2(u(I+\tfrac{1}{2}, J) - u(I-\tfrac{1}{2}, J))^2/(\Delta x)^2 + 2(v(I, J+\tfrac{1}{2}) - v(I, J-\tfrac{1}{2}))^2/(\Delta y)^2\\
&\quad + \tfrac{1}{4}[(v(I+1, J+\tfrac{1}{2}) - v(I, J+\tfrac{1}{2}))/\Delta x + (u(I+\tfrac{1}{2}, J+1) - u(I+\tfrac{1}{2}, J))/\Delta y]^2\\
&\quad + \tfrac{1}{4}[(v(I, J+\tfrac{1}{2}) - v(I-1, J+\tfrac{1}{2}))/\Delta x + (u(I-\tfrac{1}{2}, J+1) - u(I-\tfrac{1}{2}, J))/\Delta y]^2\\
&\quad + \tfrac{1}{4}[(v(I, J-\tfrac{1}{2}) - v(I-1, J-\tfrac{1}{2}))/\Delta x + (u(I-\tfrac{1}{2}, J) - u(I-\tfrac{1}{2}, J-1))/\Delta y]^2\\
&\quad + \tfrac{1}{4}[(v(I+1, J-\tfrac{1}{2}) - v(I, J-\tfrac{1}{2}))/\Delta x + (u(I+\tfrac{1}{2}, J) - u(I+\tfrac{1}{2}, J-1))/\Delta y]^2\}^{1/2}.
\end{aligned}
$$

For extension to the three dimensions actually utilized, the additional terms on the right to be included are the similar finite-difference counterparts of $2(\partial w/\partial z)^2$, $(\partial w/\partial y + \partial v/\partial z)^2$ and $(\partial u/\partial z + \partial w/\partial x)^2$.

REFERENCES

1. J. W. DEARDORFF, A numerical study of three-dimensional turbulent channel flow at large Reynolds numbers, *J. Fluid Mech.* **41** (1970), 453–480.
2. J. W. DEARDORFF, A three-dimensional numerical investigation of the idealized planetary boundary layer, *Geophys. Fluid Dynamics* **1** (1970), 377-410.
3. J. W. DEARDORFF AND R. L. PESKIN, Lagrangian statistics from numerically integrated turbulent shear flow, *Phys. Fluids* **13** (1970), 584–595.
4. D. K. LILLY, The representation of small-scale turbulence in numerical simulation experiments, *in* "Proceedings of the IBM Scientific Computing Symposium on Environmental Sciences," IBM Form No. 320-1951, 1967.
5. J. S. SMAGORINSKY, General circulation experiments with the primitive equations: I. The basic experiment, *Mon. Weather Rev.* **91** (1963), 99–164.
6. S. POND, R. W. STEWART, AND R. W. BURLING, Turbulence spectra in the wind over waves, *J. Atmos. Sci.* **20** (1963), 319–324.
7. D. K. LILLY, "On the Application of the Eddy Viscosity Concept in the Inertial Subrange of Turbulence," National Center for Atmospheric Research, Boulder, Colo., Manuscript No. 123, 1966.
8. P. D. LAX AND B. WENDROFF, Systems of conservation laws, *Comm. Pure Appl. Math.* **13** (1960), 217–237.
9. F. H. HARLOW AND J. E. WELCH, Numerical calculation of time-dependent viscous incompressible flow of fluid with free surface, *Phys. Fluids* **8** (1965), 2182–2189.
10. P. D. THOMPSON, "Numerical Weather Analysis and Prediction," MacMillan Co., New York, 1961.
11. C. W. HIRT, Heuristic stability theory for finite-difference equations, *J. Comp. Phys.* **2** (1968), 339–355.
12. D. K. LILLY, On the computational stability of numerical solutions of time-dependent nonlinear geophysical fluid dynamics problems, *Mon. Weather Rev.* **93** (1965), 11–26.
13. G. P. WILLIAMS, Numerical integration of the three-dimensional Navier–Stokes equations for incompressible flow, *J. Fluid Mech.* **37** (1969), 727–750.
14. A. ARAKAWA, Computational design for long term numerical integration of the equations of fluid motion. Two-dimensional incompressible flow. Part 1. *J. Comp. Phys.* **1** (1966), 119–143.
15. G. FISCHER, A. survey of finite-difference approximations to the primitive equations, *Mon. Weather Rev.* **93** (1965), 1–10.
16. J. LAUFER, "Investigation of Turbulent flow in a Two-Dimensional Channel," NACA Report 1053, 1950.
17. J. A. BUSINGER, Transfer of momentum and heat in the planetary boundary layer, *in* "Proceedings of the Symposium on Arctic Heat Budget and Atmospheric Curculation," RM-5233-NSF, Rand Corp., 305, 1966.
18. J. L. LUMLEY AND H. A. PANOFSKY, "The Structure of Atmospheric Turbulence," Wiley (Interscience), New York, 1964.
19. D. LENSCHOW, Airplane measurements of planetary boundary layer structure, *J. Appl. Meteorol.* **9**, No. 6, 1970.

20. F. PASQUILL, "Atmospheric Diffusion," D. Van Nostrand, Princeton, N. J., 1962.
21. D. LENSCHOW AND W. B. JOHNSON, Concurrent airplane and balloon measurements of atmospheric boundary layer structure over a forest, *J. Appl. Meteorol.* **7** (1968), 79–89.
22. R. H. KRAICHNAN, Dispersion of particle pairs in homogeneous turbulence, *Phys. Fluids* **9** (1966), 1937–1943.